Lafia Journal of Scientific & Industrial Research (LJSIR), Vol. 1(1&2), 2023
e-ISSN:... p-ISSN: 3026 – 9288 pages 1-7
https://lafiascijournals.org.ng/index.php/ljsir/ ⇒ Published by the Faculty of Science,
Federal University of Lafia, Nasarawa State, Nigeria

Proton Beam Therapy-based Computation in the Treatment of Human Ovarian and Liver Cancer Using SRIM

Joseph Omojola*, Johnson Akinade Bamikole & Olodu Ali
Department of Physics, Federal University Lafia, Nigeria

Abstract

Proton beam therapy is a promising technique used to cure various types of cancer diseases in the human body. This technique can selectively damage cancer cells while leaving surrounding cells unaffected thereby minimizing collateral damage to the healthy cells. The position and the width of the cancerous cells are determined to calculate the energy required to destroy the affected cells. The energy loss to the damaged cells and other body parts is calculated separately with high accuracy. Computational analysis indicates that proton beams with energies of 46 MeV, 47 MeV, and 48 MeV effectively destroy localized cancerous cells of the ovary from the epithelial cells to the more invasive cancerous growth while proton beam energy range of 50 MeV to 89 MeV should be considered for the treatment of liver cancer of both the periphery tumours and tumours in the hilum. Transport of ions in matter (TRIM) data shows that more than 80% of proton energy is given off during ion bombardment at Bragg's peak, while the remaining percentage is lost by phonon production and by recoils.

Keywords: Proton Beam Therapy, SRIM, human ovary, human liver, carcinoma

Article History

Submitted
July 13, 2023

Revised
October 3, 2023

First Published Online
October 29, 2023

Corresponding author
J. Omojola ✉
omojola.josef@gmail.com

doi.org/10.62050/ljsir2023.v1n1.166

Introduction

Proton beam therapy (PBT) is a particle therapy technique that employs a proton beam to irradiate affected tissues in the human body. Owing to its excellent physical properties and dosimetry parameters, PBT has been used in a variety of cancer treatments for example Wilson proposed PBT for the first time in 1946 [1]. Researchers at the Lawrence-Berkeley National Laboratory published the first PBT case series after a 12-year wait. Several other proton treatment facilities emerged throughout the world during the next few decades, and PBT has now been utilized in the clinical environment for more than 60 years, treating tens of thousands of patients with various forms of cancer cases. The appropriate application of PBT has led to fewer adverse effects and higher therapeutic efficacy compared with conventional radiotherapy (RT) using X-ray beams. Thus, facilities for PBT are being built worldwide, despite the requirement for costly equipment [2–4]. Over the past decades, with increasing PBT applications worldwide, the number of new programs under development has been growing. The reason for this is that the proton dose distribution that may be achieved is generally superior to the dose distribution of conventional photon radiation therapy (PRT). PBT may improve the survival rate of patients by improving the local tumour treatment rate, while reducing injury to normal organs, resulting in fewer radiation-induced adverse effects. The clinical benefits of PBT have been established in terms of fewer side effects when compared to photon treatment. However, the use of PBT is controversial due to the high treatment costs associated with proton facility development and maintenance. When compared to photon treatment, however, the higher cost may be justified because of the improved quality of life and lower expenditures associated with post-exposure illness and care. More research and discussion are needed to address the use of PBT in various malignancies, as well as how to maintain patients' quality of life while achieving a high cure rate [1, 5]. In recent decades, as the number of PBT applications around the world has grown, so has the number of new programs in development. Because the proton dosage distribution that may be achieved is generally superior to the photon dose distribution, this is the rationale. PBT can potentially improve patient survival rates by enhancing local tumour treatment rates while reducing damage to normal organs, resulting in fewer radiation-induced adverse effects. Compared to typical photon RT, heavier subatomic particles can convey their energy more accurately to the tumour, with less scattering to adjacent tissues. PBT is associated with obvious benefits, such as reducing the volume of irradiated normal tissue and improving the conform-ability and the quality of the target area. Data showed that 11.5% of proton patients experienced a grade three or higher side effect. In the photon group, 27.6% experienced a grade three or higher side effect. A weighted analysis of both patient groups, which controlled for other factors that may have led to differences between the patient groups, found that the relative risk of severe toxicity was two-thirds lower for proton patients compared to photon patients [6, 7].

Importantly, overall survival and disease-free survival were similar between the two groups, suggesting that the reduction in toxicity seen with proton therapy did not come at cost-effectiveness. Further studies and discussions are required to make proton therapy cost-effective to address its use in several types of cancer and to maintain the quality of life of patients while achieving a high cure rate.

Apart from the adverse effects of exposure to energetic particles due to carcinogenesis and degenerative disease, proton therapy in the treatment of cancer is a promising approach to curbing the growth of cancerous cells in the body [1, 7–11]. The damage (Bragg's peak) due to ionization and recoils in the target atoms during proton bombardment at a certain energy can be localized to destroy cancerous cells [4, 11]. Bragg peak is a distinct property of protons and when it reaches cancer tissues after penetrating through the normal tissues in the body, it releases an immense amount of radiation energy to kill the cancer cells and subsequently, it disappears instantly.

This work reports the stopping range of ions in matter and the energy deposition by the target atoms in the human liver and ovary when the composition of a healthy human liver and ovary in a computational phantom are bombarded with protons at varying energies using SRIM-2013 (the Stopping and Range of Ions in Matter) [5, 12]. Following this section of the study is a detailed description of the materials and methods in the computation, the composition of the targets (human liver and the ovary), and the SRIM set-up of the computation phantom. The remaining part of the article is discussed under results and discussion, and conclusion.

Materials and Methods

Human liver

The liver is the largest solid organ in the human body located under the rib cage in different configurations according to body size (Fig. 1) and plays a significant role in the vital metabolic functioning of the body these functions include removing waste products and foreign substances from the bloodstream, regulating blood sugar levels, and creating essential nutrients. During development, liver size increases with increasing age, averaging a 5 cm span at 5 years, and attaining an adult size average of about 8.6 cm (male and female) from age 15, with an average volume of 1624 cm^3 [11] and weighing about 1.5 kg. However, the size depends on several factors including age, sex, body size, shape, and to what extent the liver is healthy[13, 14].

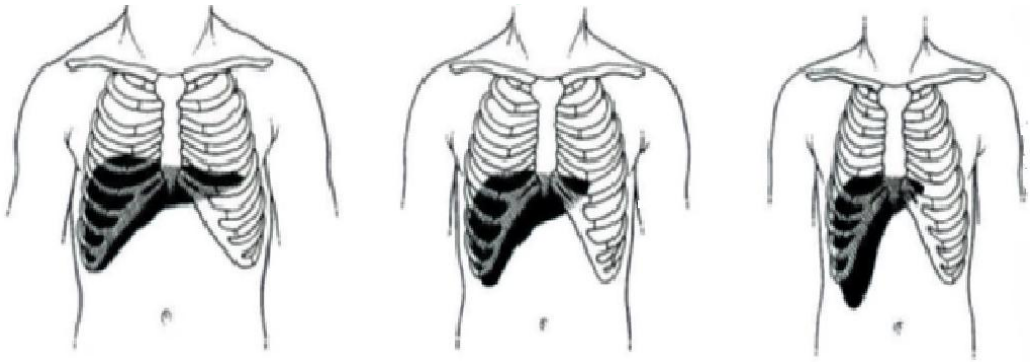

Figure 1: Different configurations of the human liver frontal view (in shaded black) in the rib cage accordingto body size [14] considered in the computational phantom.

This computation is useful for the treatment of carcinomas that originated and are localized in the liver such as hepatocellular carcinoma, intrahepatic cholangiocarcinoma and hepatoblastoma, not the ones that spread from other regions of the body.

We adopted the stoichiometry composition of the human liver from the previous work [15, 16] described in Table 1.

Table 1: Stoichiometric composition of human liver

Elements	Atomic No.	Weight (AMU)	Atomic %
Hydrogen	1	1.008	11
Carbon	6	12.01	4.1
Nitrogen	7	14.00	1.2
Oxygen	8	15.99	82.5

Table 2: Stoichiometric composition of the human skin

Elements	Atomic No.	Weight (AMU)	Atom (%)
Hydrogen	1	1.008	10.0
Carbon	6	12.01	25.0
Nitrogen	7	14.00	5.0
Oxygen	8	15.99	59.0
Sodium	11	22.99	0.20
Sulfur	16	32.06	0.30
Chlorine	17	35.45	0.30
Potassium	19	39.09	0.10

Human skin

To achieve a more realistic approach in our simulation, we have included the first layer as human skin. This skin consists of both the epidermis and dermis. We have used an average thickness of 0.138 cm, which is based on the average thickness of human skin on the abdomen and chest [17, 18] with a density of 1.09 g/cm^3. The stoichiometry of the human skin is taken from the SRIM 2013 data archive (Table 2).

Stoichiometric composition of human skin

The stoichiometric composition of human skin refers to the ratio of different elements present in the human skin [15, 17, 19]. These elements play a vital role in the structure and function of the skin. It helps determine the chemical makeup of the skin. These include carbon, oxygen, hydrogen, nitrogen, sulfur, potassium, and trace amounts of other elements.

Human ovary

The female reproductive system consists of internal organs such as the uterus, cervix, vagina, ovaries and fallopian tubes. The external structures include the breasts and labia. The ovaries are two small almond-shaped organs that lie on either side of the uterus in a depression called the ovarian fossa. They are connected to the uterus by Fallopian tubes which are hollow muscular tubes.

The ovaries' (Fig. 2) primary function is to store the ova (eggs) that a female child is born with; these ova reach maturity at puberty and every month one ovum is released during menstruation. The ova passes through the fallopian tubes into the uterus. The ovaries also produce oestrogen and progesterone which are the female hormones. They regulate menstruation and the development of sex organs. The ovary is made up of three different cell types including epithelial cells, germ cells, and stromal cells. Tumours can develop in any of these cells, when these cells become abnormal, they can divide and form tumours. These cells can also invade or spread to other parts of the body.

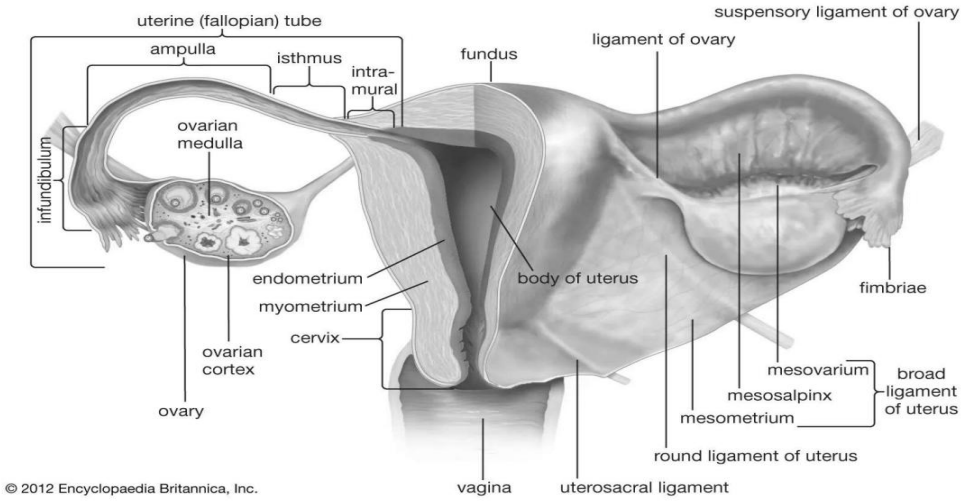

Figure 2: The female reproduction anatomy showing the ovary

The stoichiometric composition of the human ovary

The stoichiometric composition of the human ovary in Table 3 refers to the ratio of different elements present in the ovary. The human ovary is composed of various types of cells, including oocytes (egg cells) and supporting cells. They contain elements like carbon, oxygen, hydrogen, nitrogen and other trace elements [15]. The ovary is 3 cm long, 2.5 cm wide and 1.5 cm thick having a density of 0.252 g/cm^3

Table 3: The stoichiometric composition of the human ovary

Elements	Atomic No.	Weight (AMU)	Atomic %
Hydrogen	1	1.008	10.2
Oxygen	8	15.99	83.4
Carbon	6	12.01	4.6
Nitrogen	7	14.00	1.1

The stoichiometric composition of muscles equivalent

In the computational phantom of the human ovary, we introduce the International Commission on Radiation Units and Measurement (ICRU) muscle equivalent in the SRIM data archive to account for the soft tissues surrounding the ovary. The muscles equivalent has a width of 9.8 mm and 1.99 g/cm^3 density. The stoichiometric composition referred to in Table 4 is the atomic makeup, which comprises elements such as hydrogen, carbon, nitrogen and oxygen [1].

Table 4: The stoichiometric composition of muscles equivalent

Elements	Atomic No.	Weight (AMU)	Atomic %
Hydrogen	1	1.008	10.2
Carbon	6	12.01	12.0
Nitrogen	7	14.00	3.5
Oxygen	8	15.99	74.2

Stopping power and range

The Stopping power describes the energy loss per unit path length when charged particles, such as protons, propagate through matter [3, 4, 11, 20]. Charged particles lose their energy mainly through collisions with atomic electrons of the traversed medium. As a result of these collisions, the electrons can be raised to a higher shell (excitation) or ejected from the atom (ionization). The range of the proton is determined by the inelastic interactions with atomic electrons. The stopping power, *S*, can be described by the Bethe-Bloch formula,

The formula describes the particle energy loss, dE per unit path length, dx, of the traversed matter.

$$S = -\frac{dE}{dx} = 2\pi N_A r_e^2 m_e c^2 \rho \frac{z}{A}\frac{z^2}{\beta^2}\left[\ln\left(\frac{2m_e\gamma^2 v^2 W_{max}}{I^2}\right) - 2\beta^2 - \delta - 2\frac{C}{z}\right] \quad (1)$$

r_e classical electron radius given as 2.818 fm, m_e mass electron, 0.51MeV/c, Z atomic number of absorbing material, c is the speed of light, v speed of the incident particle, z charge number of incident particle, I mean excitation potential, C shell correction, N_A Avogadro's number, W_{max} Maximum energy transfer in a single collision, A atomic mass of absorbing material, ρ density, $\beta = v/c$ of incident particle, γ Lorentz factor $1/(1-\beta)^2$, δ density correction.

Energy loss rate

The energy loss rate of ions, or linear stopping power, is defined as the quotient of dE and dx, where E is the energy and x is the distance. It is frequently more convenient to express the energy loss rate in a way that is independent of the mass density; the mass stopping power is defined as

$$\frac{S}{\rho} = -\rho\frac{dE}{dx} \quad (2)$$

where ρ is the mass density of the absorbing material. Stopping power is defined as a beam, not a particle. The energy loss rate may be described by several mathematical formulae. The simplest, yet still remarkably accurate, formula is based on the Bragg-Kleeman (BK) Rule which was originally derived for alpha particles and is given by

$$\frac{S}{\rho} = -\rho\frac{dE}{dx} \approx -\frac{U^{1-\rho}}{\rho\alpha p} \quad (3)$$

where ρ is the mass density of the material, α is a material-dependent constant, U is the initial energy of the proton beam, and the exponent p is a constant that considers the dependence of the proton's energy or velocity. Values of α and p may be obtained by fitting to either ranges or stopping power data from measurements or theory. By integrating the reciprocal of the stopping power in Equation 1 we obtained the average range (R) in Equation 4.

$$R = \int_0^U \left(\frac{dU}{dx}\right)^{-1} dE \approx \sum_0^E \left(\frac{dE}{dx}\right)^{-1} \Delta E \quad (4)$$

The range is dependent on the proton energy and the characteristics of the biological matter.

SRIM set-up

Here we describe the physical model of the SRIM set-up for the TRIM (the Transport of Ions in Matter) calculations of our sample (Fig. 2). To achieve consistency in the calculation and low uncertainty, we used 10,000 incident ions. This is a good compromise between accuracy and computation time.

The energy transferred to the recoil and the ionization data files were used to calculate the energy deposited per target depth at the Bragg's peak (T_{dep}) (Eqn. 5).

$$T_{dep}/depth = (E_{recoil} - E_{ioniz}) \times 10000 \quad (5)$$

The effective displacement energy ($E_d{}^{eff}$) of the targets is calculated using Equation 6.

$$E_d{}^{eff} = \left[\sum_n \frac{S_n}{E_{d,n}}\right]^{-1} \quad (6)$$

where $E_{d,n}$ and S_n are the displacement energyand the stoichiometry fraction of the nth ions, respectively (Tables 5 and 6) [2, 21].

The default SRIM surface binding energy (≤ 8 eV) (Table 6) was used during all calculations with lattice binding energy (3 eV). The computational set-up of the layers is shown in Figs. 3 and 4.

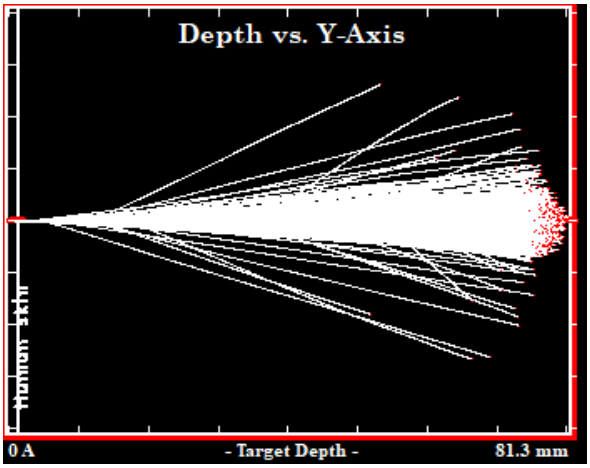

Figure 3: SRIM simulation on the human skin + liver layerswhere the white streaks represent the proton beam paths,and the red dots are the recoiling atoms

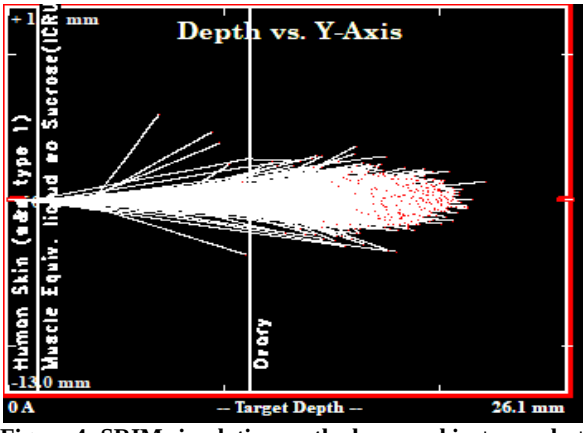

Figure 4: SRIM simulation on the human skin + muscle + ovary layers where the white streaks represent the proton beam paths, and the red dots are the recoiling atoms

Table 5: Displacement energy ($E_{d,n}$) of the constituents' atoms

	H	C	N	O	S	Cl	Na	K	E_d^{eff}
eV	10	28	28	28	25	25	25	25	11.77

Table 6: Surface binding energy of the constituents' atoms

	H	C	N	O	S	Cl	Na	K
eV	2.00	7.41	2.00	2.00	2.88	2.00	1.12	0.93

Results and Discussion

SRIM's quick calculation of damage, or Q-C, only tracks the targeting ion up to the initial impact of the projectile on the target. While this can provide insight into the primary effect of protons on the target ions, it doesn't account for the secondary ions due to recoils and collisions that occur when the projectile interacts with the atomic species in the target. To account for the secondary and tertiary ions due to recoils we run the SRIM code in the full cascade (F-C) mode.

Proton beam on liver computation

When a proton is directed towards a target, it releases its energy at a specific depth, known as the Bragg's peak. This is the targeted area of the tumour. More than 80% of the proton's energy is deposited at this point, while the remaining percentage goes to the recoil ions. However, at 20 MeV, the energy deposited at the Bragg's peak is less than 50%, and it does not penetrate beyond the skin layer. Thus, depending on the location and depth of the affected area, proton beam therapy with energies ranging from 50 MeV to 89 MeV is enough to treat liver carcinoma cells of both the peripheral and hilum tumours.

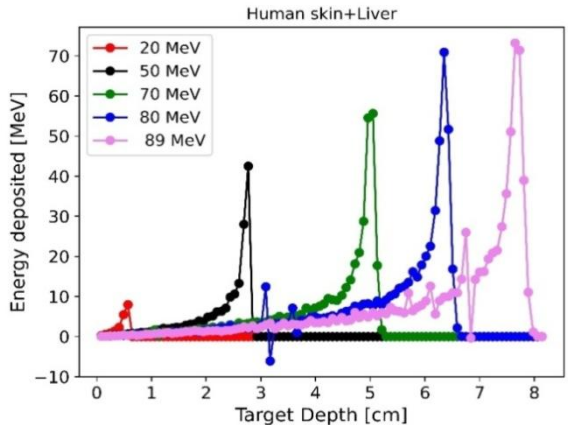

Figure 5: Proton beam energy deposition (T_{dep}) per Target depthof the human liver at different energies showing the Bragg peaks

Proton of 50 MeV as a stopping range of less than 3 cm (Table 7) into the target layers could be used for the treatment of the epithelial scarring of the liver in the periphery tumour with little to non-damage to the surrounding organs and tissues; while proton at higher energies (60 MeV to 89 MeV) could be effective against deep-rooted liver carcinoma (Table 7). The property and the characteristic Bragg's peak as shown in Fig. 5 makes PBT a very promising method in the treatment of cancer cells in the body that will preserve the surrounding healthy cells.

Table 7: The stopping range and straggle of the proton ions on the liver

Energy (MeV)	Proton range (cm)	Straggle (cm)
50	2.72	0.0001
70	4.99	0.064
80	6.35	0.081
89	7.68	0.130

Proton beam on ovary computation

The ovary is located within soft tissues and muscles in the body, unlike the liver which is not. Because of this, we include the muscle-equivalent soft tissues of the ICRU in our computational phantom. The computation results in Figs. 6 and 7 show a unique double Bragg's peaks - one within the soft tissue around the ovary, and the other within the ovary itself. The first peak indicates that a significant amount of energy is deposited in the soft tissue, specifically 20% of the proton energy. This energy is higher at 46 MeV (30% of proton energy) and lower at 48 MeV (less than 20%). This suggests that it is crucial to determine the location and the depth of the affected organ to estimate the accurate stopping power and range of the PBT and the energy requirement for the treatment. This will help minimize the collateral damage to the surrounding tissues when using PBT as a treatment for ovarian cancer.

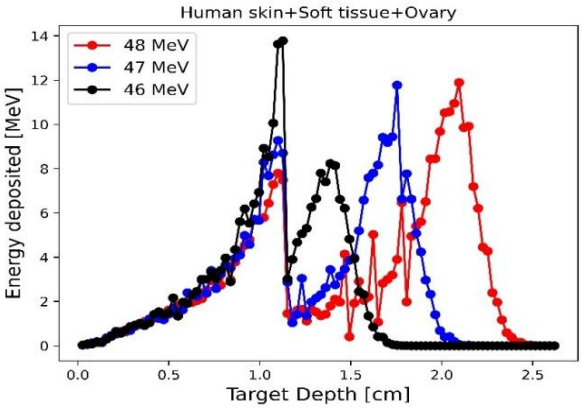

Figure 6: Proton beam energy deposition (T_{dep}) per Target depth of the human ovary at different energies showing the Bragg peaks at 46 MeV, 47 MeV, and 48 MeV

The ranges in Table 8 are where the Bragg peak occurs whereby the proton deposited the highest energy that can destroy the localised cancer cells in the ovary for example in Fig. 6 this occurs at the second peak consistent with **t**he location of the ovary.

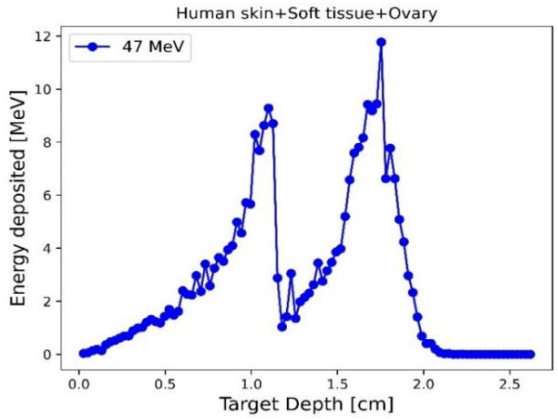

Figure 6: Proton beam energy deposition (T_{dep}) per Target depth of the human ovary at 47 MeV

Table 8: The stopping range and straggle of the proton ions on the ovary

Energy (MeV)	Proton range (cm)	Straggle (cm)
46	1.39	0.107
47	1.73	0.115
48	2.07	0.119

Conclusion

According to our calculations, SRIM is suitable for estimating the amount of proton energy needed, proton stopping range, and deposition energy required for proton beam therapy (PBT) in the treatment of liver and ovarian cancer [1]. PBT is particularly useful in treating localized tumours. In the liver computation phantom, over 80% of the projectile energy is deposited at Bragg's peak, whereas the ovary computation shows a double peak with only 20% or less of the energy deposited in the soft tissues and muscle surrounding the ovary. At 46 MeV, a higher percentage of proton energy is deposited within the tissues compared to higher energies (47 MeV and 48 MeV) for the ovary computation. This means that proton energy between 46 MeV and 48 MeV can be used to treat various types of ovarian tumours. However, it is important to protect the surrounding tissues from collateral damage that may prolong the patient's recovery period, especially at low energy.

Overall, proton energy within the range of 50 MeV to 89 MeV is useful for treating liver cancer, while proton energy within the range of 46 MeV to 48 MeV is suitable for treating ovarian cancer. Beyond these energy ranges, most of the protons will be completely transmitted through the computation phantom without interacting with the target. Since experimenting with living tissues and organs can be challenging, using a simple theoretical model like the one we use here is essential for studying the energy requirement and dose distribution to be used in proton beam therapy before attempting the real treatment.

Conflicts of interest: The authors declare no conflict of interest nor any competing interest in the manuscript.

Acknowledgement: We acknowledge that this research did not receive any specific grants from public, commercial, or not-for-profit sectors.

References

[1] Giri, K. Khatiwada, A. and Bista, P. (2022). SRIM as a computational tool to study energy required during prostate cancer treatment. *J. Nepal Phys. Soc.*, 8(1), 48–54, doi: 10.3126/jnphyssoc.v8i1.48285.

[2] Agarwal, S., Lin, Y., Li, C., Stoller, R. E. and Zinkle, S. J. (2021). On the use of SRIM for calculating vacancy production: Quick calculation and full-cascade options. *Nucl. Instrum. Methods Phys. Res. Sect. B Beam Interact. Mater. At.*, 503, 11–29, doi: 10.1016/j.nimb.2021.06.018.

[3] Zacharatou Jarlskog, C. and Paganetti, H. (2008). Physics settings for using the Geant4 toolkit in proton therapy. *IEEE Trans. Nucl. Sci.*, 55(3), 1018–1025, doi: 10.1109/TNS.2008.922816.

[4] Zinkle, S. J. and Snead, L. L. (2018). Opportunities and limitations for ion beams in radiation effects studies: Bridging critical gaps between charged particle and neutron irradiations. *Scr. Mater.*, vol. 143, 154–160, doi: 10.1016/j.scriptamat.2017.06.041.

[5] Stoller, R. E., Toloczko, M. B., Was, G. S., Certain, A. G., Dwaraknath, S. and Garner, F. A. (2013). On the use of SRIM for computing radiation damage exposure. *Nucl. Instrum. Methods Phys. Res. Sect. B Beam Interact. Mater. At.*, 310, 75–80, doi: 10.1016/j.nimb.2013.05.008.

[6] Chen, S. and Bernard, D. (2020). On the calculation of atomic displacements using damage energy. *Results Phys.*, 16, 102835, doi: 10.1016/j.rinp.2019.102835.

[7] Chung, C. S., Yock, T. I., Nelson, K., Xu Y., Keating, N. L. and Tarbell, N. J. (2013). Incidence of second malignancies among patients treated with proton versus photon radiation," *Int. J. Radiat. Oncol.*, vol. 87, no. 1, 46–52, doi: 10.1016/j.ijrobp.2013.04.030.

[8] Cucinotta, F. A. and Durante, M. (2006). Cancer risk from exposure to galactic cosmic rays: implications for space exploration by human beings. *Lancet Oncol.*, 7(5), 431–435, doi: 10.1016/S1470-2045(06)70695-7.

[9] Saha U., Devan, K. and Ganesan, S. (2018) . A study to compute integrated dpa for neutron and ion irradiation environments using SRIM-2013. *J. Nucl. Mater.*, 503, 30–41, doi: 10.1016/j.jnucmat.2018.02.039.

[10] Sekimura, N., Kanzaki, Y., Okada, S. R., Masuda, T. and Ishino, S. (1994). Cascade damage formation in gold under self-ion irradiation. *J. Nucl. Mater.*, 212–215, 160–163, doi: 10.1016/0022-3115(94)90048-5.

[11] Uchinami, Y., Katoh N., Suzuki R., Kanehira T., Tamura M., Takao S., Matsuura T., Miyamoto N., Fujita Y., Koizumi F., Taguchi H., Yasuda K., Nishioka K., Yokota I., Kobashi K., and Aoyama H. (2022). A study on predicting cases that would benefit from proton beam therapy in primary liver tumors of less than or equal to 5 cm based on theestimated incidence of hepatic toxicity," *Clin. Transl. Radiat. Oncol.*, 35, 70–75, doi: 10.1016/j.ctro.2022.05.004.

[12] Ziegler, J. F. (1984). The stopping and range of ions in solids. *Ion Implantation Science and Technology* (Elsevier), 51–108, doi: 10.1016/B978-0-12-780620-4.50007-0.

[13] Seppelt D., Ittermann T., Kromrey M. L., Kolb C., vWahsen C., Heiss P., Völzke H., Hoffmann R. T., and Kühn J. P. (2022). Simple diameter measurement as predictor of liver volume and liver parenchymal disease. *Sci. Rep.*, 12(1), 1257, doi: 10.1038/s41598-022-04825-8.

[14] Wolf, D. C. (1990). 94 Consistency of the Liver.

[15] Kim, Y. S. (1974). Human tissues: Chemical composition and photon dosimetry data. *Radiat. Res.*, vol. 57(1), 38, doi: 10.2307/3573753.

[16] Kim, Y. S. (1974). Human tissues: Chemical composition and photon-dosimetry data. A correction. *Radiat. Res.*, 60(2), 361, doi: 10.2307/3573974.

[17] Graham, H. K., Eckersley, A., Ozols, M., Mellody, K. T. and Sherratt, M. J. (2019). Human skin: Composition, structure and visualisation methods. In *Skin Biophysics*, vol. 22, G. Limbert, Ed., in *Studies in Mechanobiology, Tissue Engineering and Biomaterials*, 22, 1–18. doi: 10.1007/978-3-030-13279-8_1.

[18] Lee, Y. and Hwang, K. (2001). Skin thickness of Korean adults.

[19] Olatunji, O. and Das, D. B. (2011). Drug delivery using microneedles. *Comprehensive Biotechnology* (Elsevier), 625–642. doi: 10.1016/B978-0-08-088504-9.00501-8.

[20] Norgett, M. J. Robinson, M. T. and Torrens, I. M. (1975). A proposed method of calculating displacement dose rates. *Nucl. Eng. Des.*, 33(1), 50–54, doi: 10.1016/0029-5493(75)90035-7.

[21] Ghoniem, N. M. and Chou, S. P. (1988). Binary collision Monte Carlo simulations of cascades in polyatomic ceramics. *J. Nucl. Mater.*, 155–157, 1263–1267, doi: 10.1016/0022-3115(88)90508-9.

Citing this Article

Omojola, J., Bamikole, J. A. & Ali, O. (2023). Proton beam therapy-based computation in the treatment of human ovarian and liver cancer using SRIM. *Lafia Journal of Scientific and Industrial Research, 1*(1&2), 1 – 7. https://doi.org/10.62050/ljsir2023.v1n1.166